Detection of spores using polarization image features and BP neural network

Yafei Wang[1,2], Ning Yang[3], Guoxin Ma[1], Mohamed Farag Taha[1,4], Hanping Mao[1*], Xiaodong Zhang[1], Qiang Shi[5]

(1. *School of Agricultural Engineering, Jiangsu University, Zhenjiang 212013, Jiangsu, China*;
2. *Jiangsu Changdian Technology Co., Ltd., Jiangyin 214400, Jiangsu, China*;
3. *School of Electrical and Information Engineering, Jiangsu University, Zhenjiang 212013, Jiangsu, China*;
4. *Department of Soil and Water Sciences, Faculty of Environmental Agricultural Sciences, Arish University, North Sinai 45516, Egypt*;
5. *School of Science and Technology, Shanghai Open University, Shanghai 200433, China*)

Abstract: Timely detection and control of airborne disease is important to improve productivity. This study proposed a novel approach that utilizes micro polarization image features and a backpropagation neural network (BPNN) to classify and identify airborne disease spores in a greenhouse setting. Firstly, disease spores were collected in the greenhouse, and their surface morphological parameters were analyzed. Subsequently, the micropolarization imaging system for disease spores was established, and the micropolarization images of airborne disease spores from greenhouse crops were collected. Then the micropolarization images of airborne disease spores were processed, and the image features of polarization degree and polarization angle of disease spores were extracted. Finally, a disease spore classification model based on the BPNN was ultimately developed. The results showed that the texture position of the surface of the three disease spores was inconsistent, and the texture also showed an irregular shape. Texture information was present on the longitudinal and transverse axes, with the longitudinal axis exhibiting more uneven texture information. The polarization-degree images of the three disease spores exhibit variations in their representation within the entirety of the beam information. The disease spore polarization angle image exhibited the maximum levels of contrast and entropy when the Gabor filter's direction was set to $\pi/15$. The recognition accuracy of cucumber downy mildew spores, tomato gray mildew spores, and cucumber powdery mildew spores were 75.00%, 83.33%, and 96.67%, respectively. The average recognition accuracy of disease spores was 86.67% based on BPNN and micropolarization image features. This study can provide a novel method for the detection of plant disease spores in the greenhouse.

Keywords: greenhouse, spores, micropolarization image, BPNN, image processing, detection
DOI: 10.25165/j.ijabe.20241705.8873

Citation: Wang Y F, Yang N, Ma G X, Taha M F, Mao H P, Zhang X D, et al. Detection of spores using polarization image features and BP neural network. Int J Agric & Biol Eng, 2024; 17(5): 213–221.

1 Introduction

There has been a growing demand for "vegetable basket" projects in recent years due to individuals' aspirations for an improved quality of life[1,2]. Currently, China boasts a protected cultivation area of over 4.2 million hm^2, extensively dispersed throughout the country, securing its position as the global leader in this domain[3,4]. The vegetable basket project in China is widely regarded as a crucial pillar of support and a significant avenue for farmers to enhance their revenue[5,6]. Tomatoes and cucumbers enjoy considerable popularity among customers because of their flavorful profiles and high nutritional content. Moreover, the cultivation space dedicated to these crops constitutes a substantial portion of China's protected agriculture area[7,8]. The greenhouse's temperature and humidity conditions are conducive to the prevalence of airborne fungal diseases[9,10]. The prevalence of airborne fungal infections is anticipated to rise annually due to the growth of cultivated areas and the prolonged practice of continuous cropping. This escalation in fungal diseases can significantly reduce crop production, ranging from 20% to 50%, and in extreme cases, complete crop failure[11]. Hence, timely detection and prevention of airborne diseases in greenhouses hold significant importance.

At present, the diagnosis of plant diseases is mainly based on the experience of producers and the results of routine laboratory or field tests. Laboratory detection technology mainly encompasses electron microscope detection technology, PCR, and molecular biological detection technology. These detection techniques can accurately determine the type of plant disease, but laboratory detection techniques have the disadvantages of being disruptive and time-consuming[12]. Conventional field detection techniques mainly use spectral and image processing techniques to detect known or

Received date: 2024-02-22 **Accepted date:** 2024-09-12
Biographies: **Yafei Wang**, PhD, Lecturer, research interest: intelligent agricultural equipment and technology, Email: wangyafei918@126.com; **Ning Yang**, PhD, Professor, research interest: intelligent agricultural equipment and technology, Email: yangning7410@163.com; **Guoxin Ma**, PhD, Lecturer, research interest: intelligent agricultural equipment and technology, Email: mgx@ujs.edu.cn; **Mohamed Farag Taha**, Postdoctoral, research interest: intelligent agricultural equipment and technology, Email: 1000006483@ujs.edu.cn; **Xiaodong Zhang**, PhD, Professor, research interest: intelligent agricultural equipment and technology, Email: zxd700227@126.com; **Qiang Shi**, PhD, Associate Professor, research interest: intelligent agricultural equipment and technology, Email: openagriculture@163.com.

***Corresponding author: Hanping Mao**, PhD, Professor, research interest: modern agricultural equipment and the Environmental control technology of facility agriculture. Department of agricultural equipment, Jiangsu University, Zhenjiang 212013, Jiangsu, China. Tel: +86-511-88790008, Email: maohpujs@163.com.

specific plant diseases. These techniques can detect plant diseases through statistical modeling inversion, and provide accurate guidance for the timely prediction and treatment of diseases in greenhouse crop cultivation[13]. Nevertheless, these diagnostic approaches cannot provide early diagnosis before the outbreak's onset. In this case, the optimal time frame for implementing crop disease control measures has already elapsed[14].

Before airborne diseases of greenhouse crops occur and spread over a large area, the first thing that happens is that the spores of airborne diseases are spread by air currents[15]. With the improvement of spore traps by technicians, more and more spore traps are now sold on the market, and using spore traps to capture airborne disease spores has become a common method[16]. The existing portable spore traps, vehicle-mounted spore traps, and fixed spore traps. Airborne disease spores are captured in the air and identified with the help of a microscope. For example, Lei et al.[17] used a portable spore catcher to collect urediniospores. Microscopic examination was conducted to capture images of urediniospores. Subsequently, the urediniospores image was processed by threshold segmentation, contour extraction, and morphological manipulation. The remote monitoring platform of urediniospores was built to collect and count wheat stripe rust spores in real-time. To identify false smut and rice blast by using microspore images, Yang et al.[18] selected four shape features and three texture features for decision tree model classification, and the detection accuracy was 94%. Wang et al.[19] extracted 90 features of spores from 600 spore data sets to establish an SVM classification model, and the overall accuracy was 92%. In order to determine the density and quantity of anthrax spores in microscope images automatically, Zhao et al.[20] proposed an image segmentation method. The experimental results demonstrate that their method achieves 93.0% mean IoU and 1.5% overall error rate. In order to address the issue of tiny targets in spore images, Zhang et al.[21] suggested a modified Yolov5-ECA-ASFF target detection algorithm. Due to the influence of the external environment, some characteristics are challenging to find in the spore images taken by ordinary optical microscopes.

Polarization imaging technology uses the polarized light reflected and scattered by various points on the surface of the detection object for imaging. Compared with the ordinary optical image, the brightness and contrast between the object and the background in the polarized image are relatively enhanced[22]. The polarization diffraction imaging approach was investigated by Jiang et al.[23] to achieve the precise classification of malignant and benign cancers. By extracting morphology-related "fingerprints", the diagnosis and early warning of tumors can be significantly improved. Feng et al.[24] developed a non-staining labeled apoptosis detection method using polarization diffraction imaging techniques, achieving a test accuracy of more than 90% on independent data sets. Feng et al.[25] used polarization diffraction technology to complete the classification experiment of Jurkat cells, Ramos cells, and other cells, and the classification effect reached 99.9%. The surface of the spores is not smooth and are some convexes. The recognition rate of spores based on surface texture information under an optical microscope is easily disturbed by the external environment. The polarization image can contain the surface microstructure information of the spores. Therefore, it is possible to classify the greenhouse crop airborne disease spores based on micropolarization image features.

This study developed a novel classification approach for classifying and identifying airborne disease spores in a greenhouse using micro polarization image features combined with BPNN. Hence, the main objectives of this study were: 1) Initially, to construct a micropolarization imaging device to capture micropolarization images of disease spores; 2) Subsequently, to process and extract the features of micropolarization images of disease spores; 3) Finally, to classify the disease spores using the developed machine learning algorithm. This study can provide a new method for the detection of plant disease spores in the greenhouse.

2 Materials and methods

2.1 Cultivation and parameter measurement of disease spore samples

1) Cultivation of disease spore samples

Cucumber and tomato plants were cultivated in a Venlo-type greenhouse at Jiangsu University, Zhenjiang, Jiangsu, China, to obtain the disease spores samples. The tomato variety tested was "Zhejiang Powder 202" (Zhejiang Yinong Seed Industry Co., Ltd., China). The cucumber variety tested was "Jinyou No. 1" (developed by Tianjin Academy of Agricultural Sciences, China). In order to obtain a sample of crop disease spores, pesticides are not sprayed during the planting of the sample. The planting of tomato and cucumber plants is shown in Figure 1.

a. Tomato plant sample b. Cucumber plant sample

Figure 1 Examples of experiment sample cultivation

Fresh diseased leaves were collected from infected cucumber plants after natural disease. Individual cucumber downy mildew and powdery mildew spots with sufficient incidence and distance from other spots were cut with scissors. Dip in sterile water, spot down and gently apply to pre-planted cucumber leaves. Spores of cucumber downy mildew and powdery mildew could not be cultured in vitro, in order to preserve the samples, these spores were transferred from old infected cucumber plants to newly cultivated cucumber plants. Then to achieve the purpose of expanding propagation and culture[26].

To obtain an uncontaminated sample of tomato gray mold spores, a leaf with diseased spots was first cut from an infected tomato plant, dipped in sterile water, and then attached to a non-infected tomato plant with diseased spots facing downwards. Repeat until the gray mold is the only spot on the tomato plant. Then, tomato leaves with gray mold were placed in the PDA (Potato Dextrose Agar) medium. The preservation and propagation of the strains were carried out.

2) Surface morphological parameters analysis of disease spore samples

Disease spores samples from PDA medium dish with sterile water were washed off. Then, spore suspension and put in a disposable test tube has been Prepared. After that, the supernatant of spore suspension was sucked by a disposable pipette and dripped into the cell counting plate. The surface morphology of the diseased

spores was observed by a three-dimensional ultra-depth-of-field microscope (VHX-900F, KEYENCE Co, Japan) in 3D display mode (Figure 2).

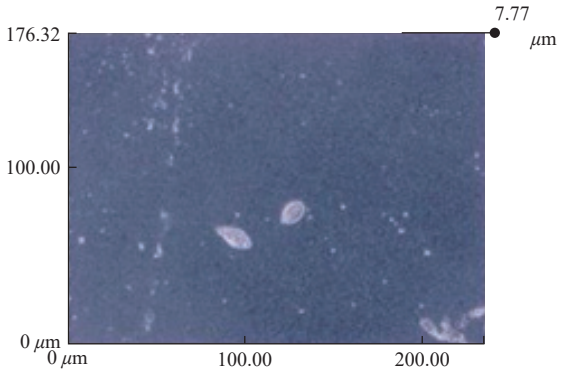

Figure 2 3D image of disease spores

2.2 Quantitative characterization method of polarization information

As a kind of electromagnetic wave, light has many characteristics. The polarization information carries the target object's delicate structure and morphological characteristics. This information and characteristics are often not available by ordinary optical measurement methods[27]. When studying polarization imaging, the relevant researchers will give priority to using the Stokes vector method[22]. Stokes vector method is used in this study. The relationship formula of the Stokes vector method was as follows:

$$S = \begin{bmatrix} S_0 \\ S_1 \\ S_2 \\ S_3 \end{bmatrix} = \begin{bmatrix} I_0 + I_{90} \\ I_0 - I_{90} \\ I_{45} - I_{135} \\ I_{\text{right}} - I_{\text{left}} \end{bmatrix} \tag{1}$$

where, S_0 represents the total optical field strength of the incident light; S_1 represents the difference in intensity between the linear polarization at 0° and 90°; S_2 represents the intensity difference between the linear polarization at 45° and 135°; S_3 represents the difference in intensity between the right and left rotation of circular polarization; I_0 represents the polarization angle is 0°; I_{45} represents the polarization angle is 45°; I_{90} represents the polarization angle is 90°; I_{135} represents the polarization angle is 135°; I_{right} represents right-hand circular polarization; I_{left} represents left-hand circular polarization.

Besides light intensity, the degree of polarization (DOP) and angle of polarization (AOP) are also commonly used to represent the polarization characteristics of light[28]. The degree of polarization was used to represent the proportion of the polarization information in the entire beam. The calculation formula was as follows:

$$\text{DOP} = \frac{\sqrt{S_1^2 + S_2^2 + S_3^2}}{S_0} \tag{2}$$

As can be seen from Equation (2), the higher the light intensity of the polarization part, the higher the value of the polarization degree. Because the polarized image contains polarization information, the more information the polarized image contains, the stronger the polarization characteristics of the polarized image of the diseased spores.

In addition, the polarization angle is the angle between the vibration direction of the polarized light and the reference direction and can also be used to represent the polarization information of disease spores. The calculation formula was as follows:

$$\text{AOP} = \frac{1}{2}\arctan\frac{S_2}{S_1} \tag{3}$$

2.3 Disease spores micro polarization image acquisition system

The polarizing images of disease spores were collected in the Bioinformatics Analysis Laboratory for the School of Agricultural Engineering, Jiangsu University. The equipment is the microscopic polarization system built by the laboratory (as shown in Figure 3). The system mainly includes a polarized camera (LUCID Vision Labs, model TRIO5OS-QC), polarized image acquisition software (ArenaView-ArenaView2), a polarized microscope (including a light source and polarizer), and a computer.

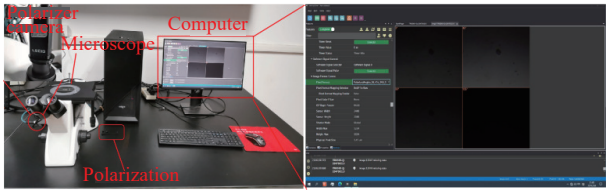

Figure 3 Disease spores micro polarization image acquisition system

2.4 Micropolarization image acquisition of disease spores

According to the previous analysis, the micropolarization images of disease spores were mainly collected at 0°, 45°, 90°, and 135° directions. The process of collecting micropolarization images of disease spores is as follows: Firstly, the disease spores were captured in the greenhouse by using a portable spore capture device, and the glass slides containing spores were put in a closed box and brought to the laboratory. Then the spores on the slide were observed under a microscope and the field of view of the spores was adjusted to the range where polarization images could be taken. Finally, the polarization image acquisition mode of the micropolarization system was opened and the disease spores were captured. The collected micropolarization images of disease spores are shown in Figures 4-6, respectively.

a. 0° b. 45° c. 90° d. 135°

Figure 4 Polarized image of tomato gray mold spores

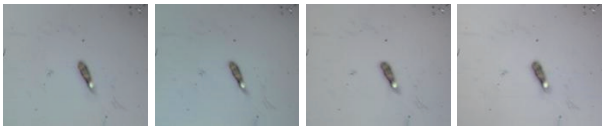

a. 0° b. 45° c. 90° d. 135°

Figure 5 Polarized image of cucumber powdery mildew spores

a. 0° b. 45° c. 90° d. 135°

Figure 6 Polarized image of cucumber downy mildew spores

2.5 Feature extraction from micro polarization images of diseased spores

1) Relative light intensity distribution value of disease spore polarization degree image

The polarization image of disease spores can be used to reflect

the proportion of their polarization information in the whole beam information. This study used a micropolarization system to capture the polarization images of diseased spores. The brightness of the light source is constant. Therefore, the relative light intensity distribution of the disease spore polarization degree image can be used to express the information of the disease spore polarization degree image. The steps for extracting the relative light intensity feature of the polarization degree image of disease spores were as follows:

(1) According to Equations (1) and (2), the polarization degree image of the disease spore image was calculated and saved as a file in .bmp format.

(2) Open Matlab software, and use import data to import the polarization degree image of disease spores saved as .bmp format into Matlab software.

(3) The double () instruction was used to convert the imported image data into a double-precision data type.

(4) mesh () command was used to convert the double precision image data to generate the 3D image and the relative light intensity value of the polarization-degree image of disease spores was obtained.

2) Texture characteristics of disease spores polarization angle image

The polarization angle image can not only highlight the detailed features of the target object but also reflect the target object' s edge contour and texture details. This study mainly extracted the edge contour and texture information of the polarization angle image of disease spores. The contrast of the gray co-occurrence matrix can reflect the contribution rate of filtered disease spores polarization angle image to its texture feature analysis. Entropy can be used to reflect the energy of polarization angle images of disease spores[29]. The more the direction of the filter is consistent with the texture direction of the disease spore polarization angle image, the greater the energy output of the disease spore polarization angle image.

Moreover, within the spatial domain, certain textures present in the image may pose challenges in their detection, although their identification becomes more straightforward upon conversion to the frequency domain. Gabor transform can extract the features of different scales and directions in the frequency domain. The two-dimensional expression of the function is shown in Equation (4):

$$g_{uv}(x,y)=\frac{k^2}{\sigma^2}\mathrm{e}^{-\frac{k^2(x^2+y^2)}{2\sigma^2}}\left[\mathrm{e}^{ik\begin{pmatrix}x\\y\end{pmatrix}}-\mathrm{e}^{-\frac{\sigma^2}{2}}\right] \tag{4}$$

Among them:

$$k=\begin{pmatrix}k_x\\k_y\end{pmatrix}=\begin{pmatrix}k_v\cos\varphi_u\\k_v\sin\varphi_u\end{pmatrix} \tag{5}$$

$$k_v=2^{-\frac{v+2}{2}}\pi \tag{6}$$

$$\varphi_u=u\frac{\pi}{K} \tag{7}$$

where, $g_{uv}()$ represents two-dimensional Gabor function; v represents the wavelength of Gabor filter; u represents the direction of the Gabor kernel function; K represents the total number of directions of the Gabor kernel function; σ/k indicates the size of the Gaussian window.

2.6 Classification and recognition of disease spores based on BP neural network

In this study, 600 micropolarized images of diseased spores were used. There were 200 micropolarized images of each disease spore. In addition, 70% of the samples were used as training sets and other samples were used to test the trained network model. That is 180 micropolarized images of disease spores as a test set for the network. The number of neurons in the hidden layer was selected according to $\sqrt{n_1+n_2}+a$, where n_1 and n_2 are respectively expressed as the number of input parameters and output parameters, and $a\in[0, 10]$. The flow chart of the disease spore classification algorithm is shown in Figure 7.

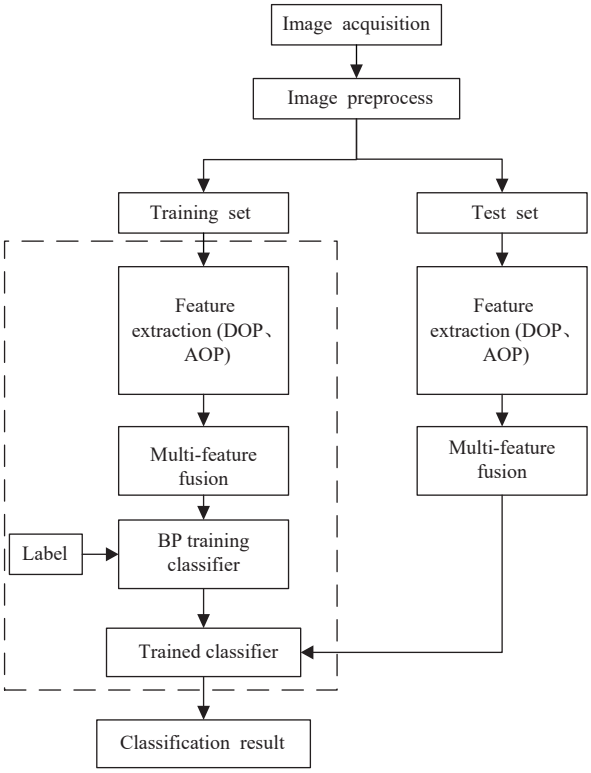

Figure 7 Process of disease spores identification and classification

3 Results and analysis

3.1 Surface morphology parameters of disease spores

According to the measurement and analysis of the surface topography parameters of the disease spores (Figure 8), the spores of tomato gray mold were round to oval, with a size range of 11.4-26.7 μm on the long axis, with an average value of 19.3 μm. The size in the direction of the short axis's direction ranges from 8.3-14.5 μm, with an average of 11.7 μm. Cucumber downy mildew spores were oval or lemon-shaped, with a size range of 21.1-39.8 μm on the long axis, with an average value of 30.6 μm. The size in the short axis's direction of 13.8-23.6 μm, with an average of 20.5 μm. The spores of cucumber powdery mildew were cylindrical and oblong, with a size of 30.2-39.5 μm, with an average value of 35.4 μm. The size in the direction of the short axis ranges from 7.3-22.2 μm, with an average of 14.2 μm.

Specifically, these spores exhibit higher concentrations in the central region and lower concentrations at both ends along the long and short-axis directions, forming a parabolic shape. The cucumber downy mildew spores had a certain depression near the top and middle of the long axis, and a V-shaped depression in the center of the short axis. In the direction of the short axis, the spores of cucumber downy mildew decreased from the beginning to 8.0 μm, and there was a trough at 8 μm. A place with three peaks and troughs along the long axis, but the spacing between the peaks and troughs is not equal. The short axis of cucumber powdery mildew

spores decreased from the beginning to 2.8 μm. There is a trough at 2.8 μm. Subsequently, the value ascends and reaches a maximum peak at 7.3 μm, then declines with a small fluctuation between 9.2 and 12.0 μm. In the longitudinal axis direction, the height of the central region can be up to 4.35 μm, surpassing the heights observed at both ends. The height at the head of the spore is close to 3.2 μm, and the height from the head to the tail of the spore fluctuates. Tomato gray mold spores decreased from the beginning to 2.0 μm along the short axis. A trough is observed at 2.0 μm, followed by a rapid rise with fluctuations between 3.0 and 5.0 μm, and a peak at 5.8 μm. A peak at 9.0 μm was seen along the longitudinal axis, while the magnitude of height fluctuation from the head to the tail of the spores was comparatively lower than that of spores belonging to cucumber powdery mildew. In summary, the texture position of the surface of the three disease spores was inconsistent, and the texture also showed an irregular shape. Texture information was observed on both the longitudinal and transverse axes, with the longitudinal axis exhibiting a greater degree of uneven texture. Hence, the disease spores can be classified based on their texture and further distinguishing features.

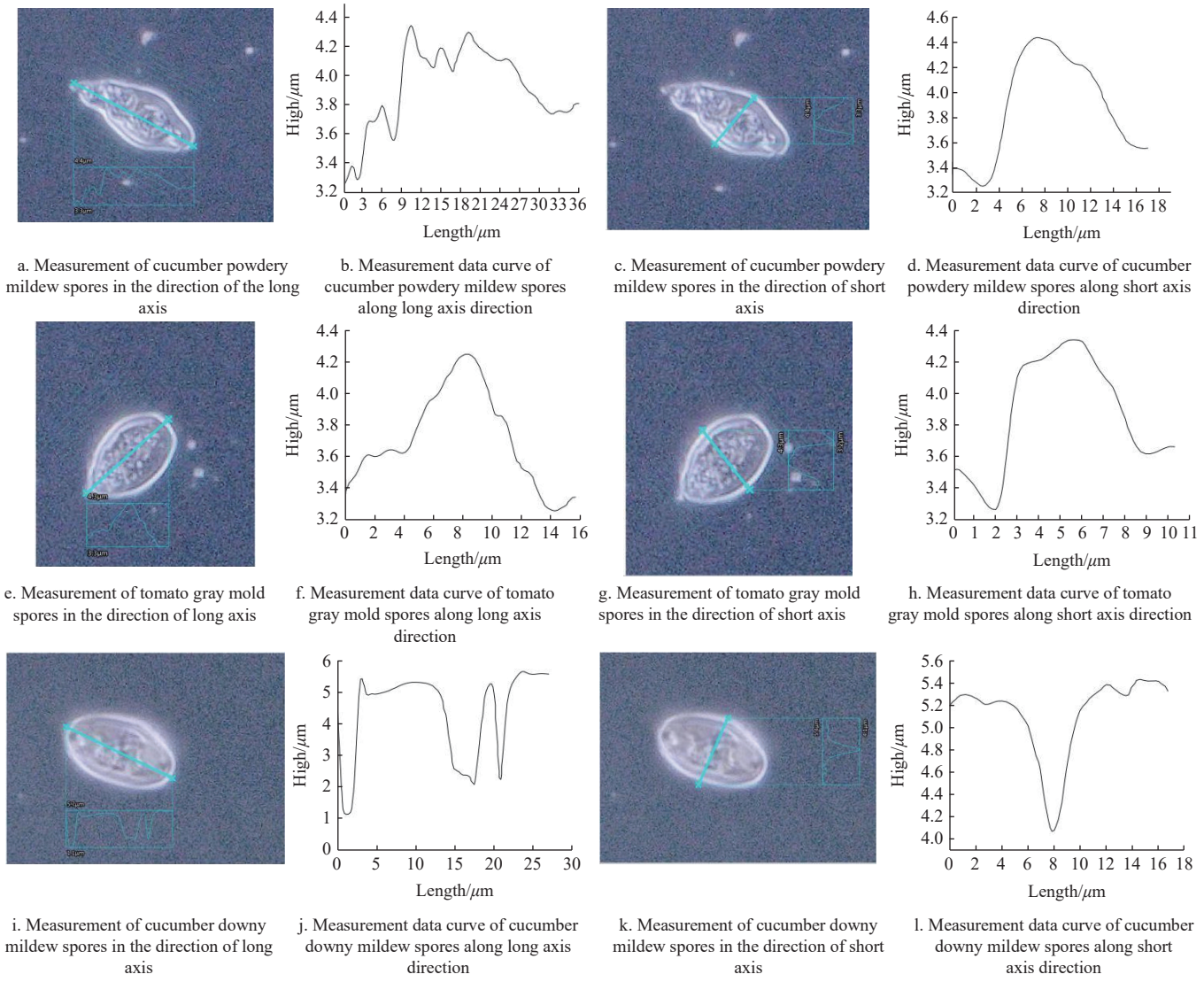

a. Measurement of cucumber powdery mildew spores in the direction of the long axis

b. Measurement data curve of cucumber powdery mildew spores along long axis direction

c. Measurement of cucumber powdery mildew spores in the direction of short axis

d. Measurement data curve of cucumber powdery mildew spores along short axis direction

e. Measurement of tomato gray mold spores in the direction of long axis

f. Measurement data curve of tomato gray mold spores along long axis direction

g. Measurement of tomato gray mold spores in the direction of short axis

h. Measurement data curve of tomato gray mold spores along short axis direction

i. Measurement of cucumber downy mildew spores in the direction of long axis

j. Measurement data curve of cucumber downy mildew spores along long axis direction

k. Measurement of cucumber downy mildew spores in the direction of short axis

l. Measurement data curve of cucumber downy mildew spores along short axis direction

Figure 8 Surface morphology parameters for three kinds of diseases spores

3.2 Processing results for diseased spores micro polarization images

According to the above analysis, Matlab R2016 b was used to write disease spores the micropolarization image processing program. The Stokes parameters (S_0, S_1, S_2, S_3), degree of polarization (DOP), and polarization Angle (AOP) images of the three disease spores were calculated as shown in Figures 9-11.

3.3 Micropolarization image features for disease spores

The relative light intensity distribution of the polarization-degree image of disease spores obtained according to the steps of feature extraction of the relative light intensity value of the polarization-degree image of disease spores is shown in Figure 12.

As can be seen from Figure 12, the relative light intensity distribution of the polarization degree image of tomato gray mold spores is more uniform than that of the other two airborne disease spores, and there are large relative light intensity values in the middle and around. The relative light intensity distribution of the polarization degree image of cucumber downy mildew spores was mainly located in the surrounding circle and showed a decreasing trend from the surrounding to the middle. The relative light intensity distribution of the polarization degree image of cucumber powdery mildew spores is mainly located in the middle, with a prominent relative light intensity value in the middle. This may be because the three disease spores have their color characteristics (the color of the tomato gray mold spores is nearly colorless, the cucumber downy mildew spores have milky white bumps on the top that are light

brown, and the cucumber powdery mildew spore is colorless). When their polarization images are taken with a micropolarization system, the spores with different color characteristics absorb and reflect the beam of light emitted by the microscope light source differently. Reflected in the polarization image of disease spores, the relative light intensity distribution of the polarization image of spores with different color characteristics is different. Therefore, the relative light intensity of polarization degree images of disease spores can be used as their polarization degree image features to classify them.

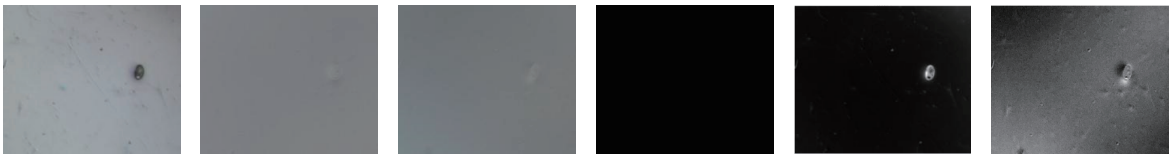

a. S_0 b. S_1 c. S_2 d. S_3 e. DOP f. AOP

Figure 9 Results for polarized image processing of tomato gray mold spores

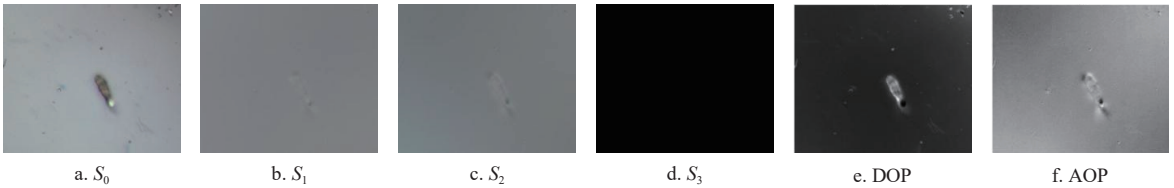

a. S_0 b. S_1 c. S_2 d. S_3 e. DOP f. AOP

Figure 10 Results for polarized image processing of cucumber powdery mildew spores

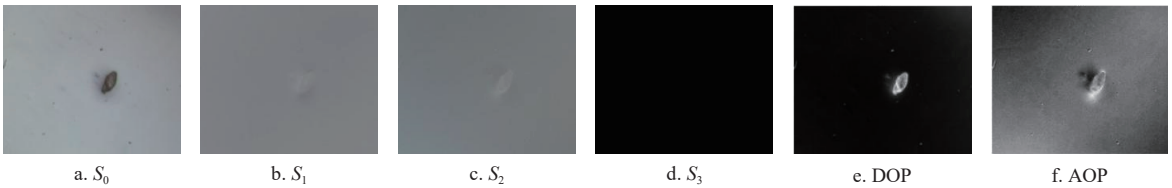

a. S_0 b. S_1 c. S_2 d. S_3 e. DOP f. AOP

Figure 11 Results for polarized image processing of cucumber downy mildew spores

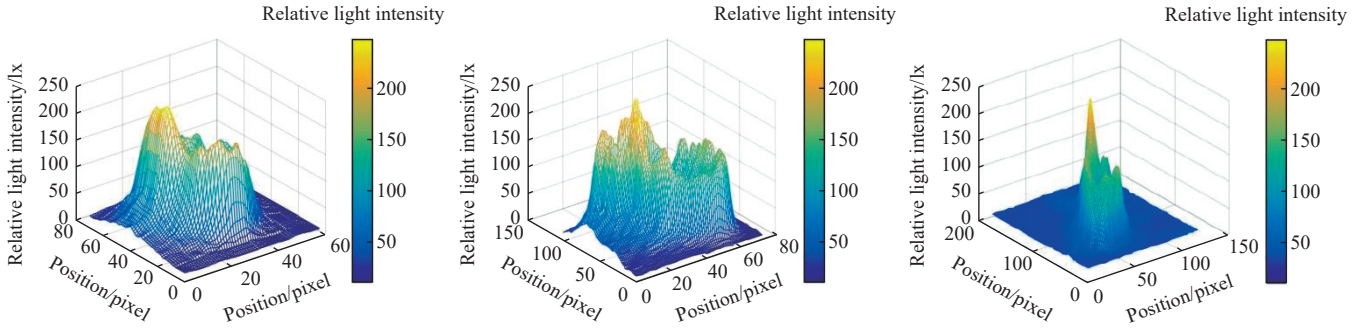

a. Tomato gray mold spores b. Cucumber downy mildew spores c. Cucumber powdery mildew spores

Figure 12 Relative light intensity distribution for the polarization degree image of disease spores

Based on the processing results of the relative light intensity distribution of disease spores' polarization degree images, the relative light intensity distribution values of the polarization degree images for three disease spores were statistically analyzed. The statistical results are listed in Table 1.

Table 1 Statistical results for relative light intensity distribution about disease spores polarization degree images

Spore species	Measured index/lx		
	Range of minimum values	Range of maximum values	Range of means
Tomato gray mold spores	12-18	163-187	82.36-87.84
Cucumber downy mildew spores	11- 15	179-205	75.27- 83.61
Cucumber powdery mildew spores	27-34	185-216	65.32-74.88

When the Gabor filter takes different directions, the contrast and entropy of the polarization Angle image of disease spores are shown in Figure 13. As can be seen from Figure 13, when the direction of the Gabor filter was π/15, the contrast and entropy of the disease spore polarization angle image were the highest. At this time, the shading degree of the disease spores' polarization angle image has the greatest contribution to its texture characteristics. The direction of the filter was also the most consistent with the texture direction of the disease spore polarization angle image. Therefore, in this study, when the Gabor filter was used to extract features in different scales and directions of polarization angle images of disease spores in the frequency domain, the direction value of the Gabor filter was set to π/15. The polarization angle image results of the treated disease spores are shown in Figure 14. By comparing Figures 14a and 14b, it can be seen that the texture information of disease spores after filtering was more clear. Therefore, according to the above analysis, the contrast and entropy of disease spores were extracted from the filtered polarization angle images of disease spores as texture features.

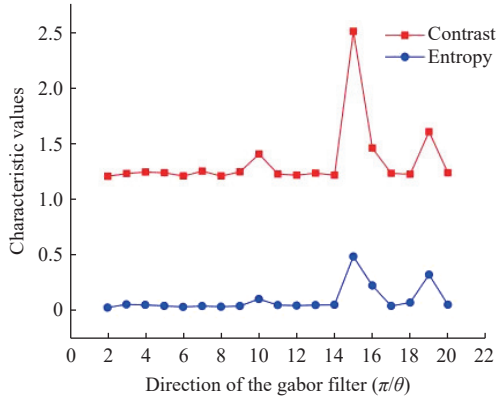

Figure 13 Effect of Gabor filter direction on contrast and entropy for polarization angle images of disease spores

3.4 Classification and identification of disease spores

In this study, 600 micropolarized images of disease spores were taken. The micropolarization images of each disease spore were 200. 30% of the data set serves as the test set for the network. That is 180 micropolarized images of disease spores as a test set for the network. The spores of cucumber downy mildew, tomato gray mold, and cucumber powdery mildew were named class 1, class 2, and class 3, respectively. The operation results of the BP neural network are shown in Figure 15.

a. Before filtering b. After filtering

Figure 14 Comparison of polarization angle images for disease spores before and after processing

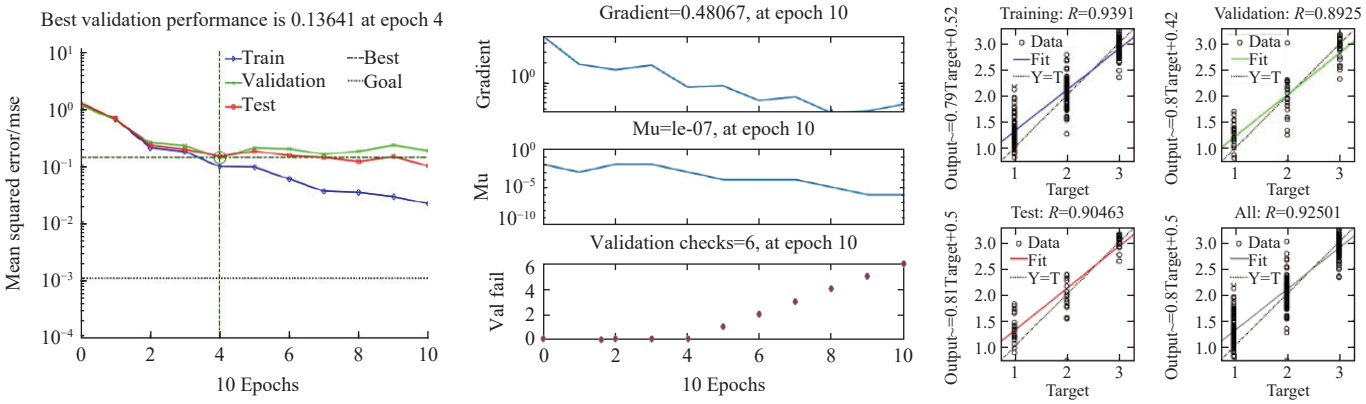

a. mean square error of different iterations b. Running status of the network c. Regression results after network training

Figure 15 Results for network operation

Using the BP neural network and micropolarization image features to classify disease spores resulted in a minimum root mean square error of 0.136 41 for the system, as depicted in Figure 15. This achievement was attained after conducting four iterations of the network. After conducting 10 iterations of the network, it was observed that the gradient of the network equaled 0.480 67. The linear coefficients of the training set, the verification set, and the test set were 0.9391, 0.8925, and 0.904 63, respectively. The performance of the network was close, and the linear coefficient of the overall network performance was 0.925 01. The classification results for the test set of three disease spores are shown in Figure 16.

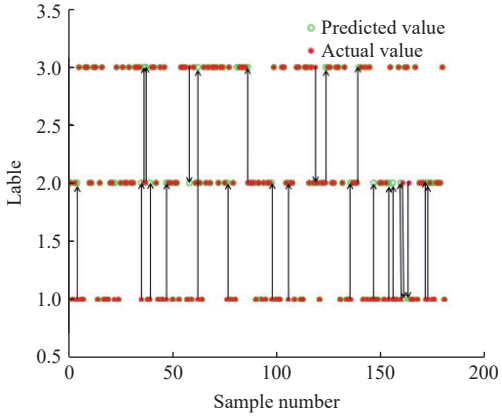

Figure 16 Classification results of three disease spore test sets

The classification results of the 180 test sets in Figure 16 were counted. The results are listed in Table 2.

Table 2 Classification results for test set

Class	Sample number	Predict the correct number of samples	Accuracy rate/%
1	60	45	75.00
2	60	53	83.33
3	60	58	96.67

According to the data presented in Table 2, the number of accurate predictions for class 1 was 45, resulting in an accuracy rate of 75%. The number of correct predictions for class 2 was 53, resulting in an accuracy rate of 83.33%. The correct prediction count for class 3 was 58, resulting in an accuracy rate of 96.67%. The mean prediction accuracy for three types of airborne disease spores was found to be 86.67%. The aforementioned results demonstrate the potential of utilizing the BP neural network and micropolarization image feature for the classification of greenhouse crop disease spores.

4 Discussion

Due to the influence of the external environment, some features of disease spores are challenging to find when taking disease spores images under visible light. The recognition rate of airborne disease spores was only 71.45% when classified based on surface texture information collected under visible light[19]. It shows that more than visible light imaging of disease spores is needed. Polarization

imaging technology can detect the polarization information of the object's surface. Compared with the ordinary optical image, the brightness and contrast of the object and the background in the polarized image are improved[22]. Different disease spores have different effects on the dispersion of polarized light, and the polarized light can also contain the surface microstructure information of disease spores. Based on this characteristic, the polarization scattering feature of different disease spores after the action of polarized light can be studied to classify the disease spores[23-25].

According to the statistical analysis of the relative light intensity distribution values of the polarization degree images of disease spores (Table 1), the relative light intensity distribution values of the three disease spores' polarization degree images are different. This may be because the spores of the three airborne diseases have their color characteristics (the color of the tomato gray mold spores is nearly colorless, the cucumber downy mildew spores have milky white bumps on the top that are light brown, and the cucumber powdery mildew spores is colorless). When their polarization images are taken with a micropolarization system, the spores with different color characteristics absorb and reflect the beam of light emitted by the microscope light source differently. The polarization angle image can highlight the detailed features of the disease spores and reflect the edge contour and texture details of the disease spores.

In this study, the maximum, minimum, and mean values of the relative light intensity distribution of the disease spore polarization degree image, the contrast, and entropy of the disease spore polarization angle image were selected as the features of the disease spore micro polarization image. The recognition rate of disease spores based on the BP neural network and micropolarization image features was lower than the average recognition accuracy (98.00%) in Reference [30]. It may be because the color features, shape features, and texture features of marigold black spot spores were selected in this paper when the BP neural network was used to identify marigold black spot spores.

In addition, the recognition rate based on the BP neural network and micropolarization image features of disease spores was lower than that based on color, shape, and texture feature fusion (94.36%). Although the same disease spores were identified, this study only considered the relative light intensity distribution of the disease spores' polarization degree, the contrast, and the entropy of the polarization angle image. The shape and color features of disease spores were not fused with the extracted micropolarization images of disease spores. But, The classification results based on BP neural network and micropolarization image features of greenhouse air-borne disease spores were much higher than those based on surface texture information of disease spores (71.45%), color information (45.68%), color and texture information fusion (75.36%), and shape and texture information fusion (86.18%)[19]. Therefore, in future research or practical applications, we can integrate the microscopic shape features of disease spores with the image features of disease spores polarization degree and angle to improve the recognition rate of disease spores.

5 Conclusions

This study proposed a novel approach to classifying and identifying airborne disease spores in a greenhouse based on micro polarization image features with a BP neural network. The texture position of the surface of the three disease spores was inconsistent, and the texture also showed an irregular shape. Texture information was present on the longitudinal and transverse axes, with the longitudinal axis exhibiting more uneven texture information. The polarization-degree images of the three disease spores exhibit variations in their representation within the entirety of the beam information. The disease spore polarization angle image exhibited the maximum levels of contrast and entropy when the Gabor filter's direction was set to $\pi/15$. The recognition accuracy of cucumber downy mildew spores, tomato gray mildew spores, and cucumber powdery mildew spores were 75.00%, 83.33%, and 96.67%, respectively. The average recognition accuracy of disease spores was 86.67% based on BPNN and micropolarization image features.

Acknowledgements

This work was partially supported by the National Natural Science Foundation of China (Grant No. 32071905, 3217895, and 32201686). A Project Funded by the Priority Academic Program Development of Jiangsu Higher Education Institutions (No. PAPD-2023-87). The National Key Research and Development Program for Young Scientists (Grant 2022YFD2000200). General Program of Basic Science (Natural Science) Research in Higher Education Institutions of Jiangsu Province(Grant 23KJB210004).

[References]

[1] Yan H F, Zhao S, Zhang C, Zhang J Y, Wang G Q, Li M, et al. Calibration and assessment of evapotranspiration methods for cucumber plants in a Venlo-type greenhouse. Irrigation and Drainage, 2024; 73(1): 119–135.

[2] Zhang C, Zhang W C, Yan H F, Ni Y X, Akhlaq M, Zhou J N, et al. Effect of micro-spray on plant growth and chlorophyll fluorescence parameter of tomato under high temperature condition in a greenhouse. Scientia Horticulturae, 2022; 306: 111441.

[3] Lakhiar I A, Gao J M, Syed T N, Chandio F A, Tunio M H, Ahmad F, et al. Overview of the aeroponic agriculture - An emerging technology for global food security. Int J Agric & Biol Eng, 2020; 13(1): 1–10.

[4] Lin J L, Ma J, Liu K, Huang X, Xiao L P, Ahmed S, et al. Development and test of an autonomous air-assisted sprayer based on single hanging track for solar greenhouse. Crop Protection, 2021; 142: 105502.

[5] Yan H F, Deng S S, Zhang C, Wang G Q, Zhao S, Li M, et al. Determination of energy partition of a cucumber grown Venlo-type greenhouse in southeast China. Agricultural Water Management, 2023; 276: 108047.

[6] Zhang C, Li X Y, Yan H F, Ullah I, Zuo Z Y, Li L L, et al. Effects of irrigation quantity and biochar on soil physical properties, growth characteristics, yield and quality of greenhouse tomato. Agricultural Water Management, 2020; 241: 106263.

[7] Huang S, Yan H F, Zhang C, Wang G Q, Acquah S J, Yu J J, et al. Modeling evapotranspiration for cucumber plants based on the Shuttleworth-Wallace model in a Venlo-type greenhouse. Agricultural Water Management, 2020; 288: 105861.

[8] Miao Y X, Luo X Y, Gao X X, Wang W J, Li B, Hou L P. Exogenous salicylic acid alleviates salt stress by improving leaf photosynthesis and root system architecture in cucumber seedlings. Scientia Horticulturae, 2020; 272: 109577.

[9] Mao H P, Wang Y F, Yang N, Liu Y, Zhang X D. Effects of nutrient solution irrigation quantity and powdery mildew infection on the growth and physiological parameters of greenhouse cucumbers. Int J Agric & Biol Eng, 2022; 15(2): 68–74.

[10] Shi Y, Yang Q Y, Zhao Q H, Dhanasekaran S, Ahima J, Zhang X Y, et al. *Aureobasidium pullulans* S-2 reduced the disease incidence of tomato by influencing the postharvest microbiome during storage. Postharvest Biology and Technology, 2022; 185: 111809.

[11] Wallace E C, D'Arcangelo K N, Quesada-Ocampo L M. Population analyses reveal two host-adapted clades of *Pseudoperonospora cubensis*, the causal agent of cucurbit downy mildew, on commercial and wild cucurbits. Phytopathology Biology, 2020; 110: 1578–1587.

[12] Riccardi C, Di Filipp.P, Pomata D, Simonetti G, Castellani F, Uccellitti D, et al. Comparison of analytical approaches for identifying airborne microorganisms in a livestock facility. Science of the Total Enviromnet,

2021; 783: 147044.

[13] Shin M-Y, Viejo C G, Tongson E, Wiechel T, Taylor P W J, Fuentes S. Early detection of Verticillium wilt of potatoes using near-infrared spectroscopy and machine learning modeling. Computers and Electronics in Agriculture, 2023; 204: 107567.

[14] Tang Z, Wang M N, Schirrmann M, Dammer K H, Li X R, Brueggeman R. Affordable high throughput field detection of wheat stripe rust using Deep Learning with Semi-Automated Image Labeling. Computers and Electronics in Agriculture, 2023; 207: 107709.

[15] Tsai M-H, Li K-T. Leaf color as a morpho-physiological index for screening heat tolerance and improved water use efficiency in rabbiteye blueberry (*Vaccinium virgatum* Aiton). Sciental Horticulturae, 2021; 278: 109864.

[16] Wang Y F, Mao H P, Xu G L, Zhang X D, Zhang Y K. A rapid detection method for fungal spores from greenhouse crops based on CMOS image sensors and diffraction fingerprint feature processing. Journal of Fungi, 2022; 8(4): 374.

[17] Lei Y, Yao Z F, He D J. Automatic detection and counting of urediniospores of *Puccinia striiformis* f. sp. tritici using spore traps and image processing. Scientific Reports, 2018; 8: 13647.

[18] Yang N, Qian Y, EL-mesery H S, Zhang R B, Wang A Y, Tang J. Rapid detection of rice disease using microscopy image identification based on the synergistic judgment of texture and shape features and decision tree - confusion matrix method. Journal of the Science of Food and Agriculture, 2019; 99(14): 6589–6600.

[19] Wang Y F, Du X X, Ma G X, Liu Y, Wang B, Mao H P. Classification methods for airborne disease spores from greenhouse crops based on multifeature fusion. Applied Sciences, 2020; 10(21): 7850.

[20] Zhao Y C, Liu S G, Hu Z H, Bai Y, Shen C, Shi X Q. Separate degree based Otsu and signed similarity driven level set for segmenting and counting anthrax spores. Computers and Electronics in Agriculture, 2020; 169: 105230.

[21] Zhang D Y, Zhang W H, Cheng T, Zhou X G, Yan Z H, Wu Y H, et al. Detection of wheat scab fungus spores utilizing the Yolov5-ECA-ASFF network structure. Computers and Electronics in Agriculture, 2023; 210: 107953.

[22] Yang L, Chen W, Bi P S, Tang H Z, Zhang F J, Wang Z. Improving vegetation segmentation with shadow effects based on double input networks using polarization images. Computers and Electronics in Agriculture, 2022; 199: 107123.

[23] Jiang W H, Lu J Q, Yang L V, Sa Y, Feng Y M, Ding J H, Hu Xinhua. Comparison study of distinguishing cancerous and normal prostate epithelial cells by confocal and polarization diffraction imaging. Journal of Biomedical Optics, 2015; 21(7): 071102.

[24] Feng J W, Sa Y. A stain-free apoptosis detection and classification method based on machine learning technique. Chinese Journal of Cell Biology, 2019; 41(7): 1371–1376.

[25] Feng Y M, Zhang N, Jacobs K M, Jiang W H, Yang L V, Li Z G, et al. Polarization imaging and classification of Jurkat T and Ramos B cells using a flow cytometer. Cytometry Part A, 2014; 85(9): 817–826.

[26] Jia Z M, Liu F, Mu W, Wei G, Liu Y L. Study on the inoculation and fungicide sensitivity assay method of Sphaerotheca on cucumber. Journal of Plant Protection, 2006; 33(1): 99–103. (in Chinese)

[27] Yu Z F, Li Y F, Deng L, Luo B, Wu P H, Geng D X. A high-performance cell-phone based polarized microscope for malaria diagnosis. Journal of Biophotonics, 2023; 16(5): e202200290.

[28] Tong L, Huang X Y, Wang P, Ye L, Peng M, An L C, et al. Stable mid-infrared polarization imaging based on quasi-2D tellurium at room temperature. Nature Communications, 2020; 11(1): 2308.

[29] Wang Y F, Zhang X D, Ma G X, Du X X, Shaheen N, Mao H P. Recognition of weeds at asparagus fields using multi-feature fusion and backpropagation neural network. Int J Agric & Biol Eng, 2021; 14(4): 190–198.

[30] Liu H, Ji R H, Qi L J, Ma W, Gao C H. Spores of marigold black spot identification based on PCA and BP neural network. Journal of China Agricultural University, 2015; 20(6): 263–268. (in Chinese)